East European Journal of Physics. 2. 508-514 (2026)
DOI:10.26565/2312-4334-2026-2-57 ISSN 2312-4334

MORPHOLOGICAL FEATURES AND MICROSTRUCTURAL CHARACTERISTICS OF CRATERS ON THE SURFACE OF INDUSTRIAL ALUMINUM ALLOY AA6111 IRRADIATED WITH A HIGH-CURRENT PULSED ELECTRON BEAM

V.V. Bryukhovetsky[1], V.V. Lytvynenko[1]*, D.E. Myla[1], O.L. Rak[2]
[1]*Institute of Electrophysics and Radiation Technologies NAS of Ukraine, 13, Gudanova Str., 61024 Kharkiv, Ukraine*
[2]*NSC «Kharkiv Institute of Physics and Technology» NAS of Ukraine, 1, Akademicheskaya Str., 61108 Kharkiv, Ukraine*
**Corresponding Author e-mail: vvlytvynenko@ukr.net*
Received March 2, 2026; revised April 20, 2026; accepted May 19, 2026

Irradiation of the industrial aluminum alloy AA6111 with a high-current pulsed electron beam (HCPEB) with particle energy of 0.35 MeV, a beam current of 2.0 kA, a pulse duration of 5 μs, and a beam diameter of 3 cm results in the formation of a surface layer with improved physical and mechanical properties. However, the potential formation of craters on the surface of HCPEB-treated materials is one of the negative effects caused by HCPEB. This study examines the types and morphology of craters formed on the surface of AA6111 aluminum alloy after irradiation with HCPEB. The distribution of crater sizes and the crater density on the irradiated surface were studied. An analysis of the elemental composition of the crater walls and the adjacent melted surface was performed. The features of the grain microstructure, including shape and size, in the crater area were studied. The implications of these observations for a deeper understanding of the mechanisms underlying crater formation during HCPEB irradiation are discussed.
Keywords: *High-current pulsed electron beam; Aluminum alloy; Surface layer; Craters*
PACS: 29.25.Bx, 61.80.Fe, 62.20.−x

INTRODUCTION

The study of the morphology and mechanisms of formation of surface structures in metals and alloys resulting from irradiation with charged-particle flows is of great scientific and applied importance. The surface treatment of solid objects by high-current pulsed electron beams (HCPEB) significantly affects their physical and mechanical properties [1-8]. High-density energy is released in the process of HCPEB-irradiation at a shallow depth below the material's surface within a short period of time. This results in rapid heating and cooling with a high temperature gradient, leading to melting, vaporization, plasma ablation, and the formation of thermal stresses and shock waves. These non-equilibrium processes can alter the microstructure, chemical composition, phase structure, and stress state at the surface. In addition, the dynamic stress field triggers intense deformation processes on the material's surface due to the HCPEB effect [9,10]. It was established that the modified cross-sectional area following HCPEB treatment is divided into three zones: the remelted layer, the heat-affected zone, and the thermal stress wave zone [11]. Metastable structures form in the molten layer due to high heating and cooling rates. The presence of crater-like defects is the most characteristic feature of the microstructure of the remelted zone [12]. Moreover, crater formation is characteristic not only of HCPEB-irradiated steels and alloys, but also of pure metals. For example, craters were observed when irradiating pure nickel, aluminum, zirconium, and copper [13-16]. The size of the craters and the density of their distribution on the irradiated surface depend on the purity of the material, grain size, irradiation parameters, and other conditions [17-19]. Crater formation increases surface roughness and creates local areas with highly inhomogeneous stress states in the near layer [17-19].

Craters form as a result of a complex set of physical processes. However, a definitive answer to the mechanisms and causes of crater formation on the HCPEB-irradiated surface has not yet been found. Issues regarding crater size and density on the irradiated surface are also debatable. Therefore, further detailed studies of crater morphological features, microstructural characteristics in the crater-formation zone, and possible mechanisms of crater formation are required. Such experimental studies are of interest not only from a technological standpoint but also from a broader scientific perspective.

MATERIAL AND EXPERIMENTAL

The studied alloy AA6111 has such a chemical composition: Al; 0,5-1,0wt.%Mg; 0,5-0,9wt.%Cu; 0,1-0,4wt.%Mn; 0,15-0,44wt.%Fe; 0,7-1,1wt.%Si; 0,15wt.%Zn; 0,1wt.%Ti [20]. The initial microstructure of the AA6111 alloy had a grain size of approximately 40 μm [21]. The grains vary in size, but there is no distinct metallographic texture. The AA6111 alloy is classified as a medium-strength aluminum alloy. Tensile strength, σ_t = 340 MPa, and yield strength, σ_y = 152 MPa [22]. The microhardness of the studied AA6111 alloy, in the initial condition, is 70*HV*0.50. The microhardness of the HCPEB-irradiated layer of the AA6111 alloy increases and on average amounts to 101*HV*0.50 [3]. The results of diffraction studies of the initial microstructure of the AA6111 alloy, reported in [3,23], revealed that the initial microstructure is characterized by the presence of phases $Al_2Fe_3Si_4$ and $Al_4Cu_2Mg_8Si_7$. The maximum elongation at break at room temperature of the AA6111 alloy under study is 21%. At elevated temperatures, despite its coarse grain size, the

Cite as: V.V. Bryukhovetsky, V.V. Lytvynenko, D.E. Myla, O.L. Rak, East Eur. J. Phys. 2, 508 (2026), https://doi.org/10.26565/2312-4334-2026-2-57
© V.V. Bryukhovetsky, V.V. Lytvynenko, D.E. Myla, O.L. Rak, 2026; CC BY 4.0 license

alloy shows superplastic behavior [21,24]. At a temperature of T = 793 K and a true strain rate, $\dot{\varepsilon} = 5{,}2 \cdot 10^{-4}$ s^{-1}, the elongation of specimens made of this alloy at break is 180%.

Plates measuring 100×100 mm^2 were cut from AA611 alloy sheets (1.2 mm thick) for irradiation. The cladding layer on the plate surface was grinded off, and the plate surface was polished before irradiation. Irradiation of alloy sheets was performed by a high-current electron beam (HCPEB) at the TEMP-A accelerator in the NSC KIPT of the NAS of Ukraine [2,3,25]. The energy flux density at the target W is approximately 10^9W/cm^2 (beam energy E ~ 0.35 MeV, current I ~ 2000 A, pulse duration τ_i ~$5 \cdot 10^{-6}$ s, beam diameter ~ 3 cm). Irradiation was done by a single impulse in a vacuum at 1.310^{-3} Pa. Microstructural examinations were conducted with an optical microscope (Olympus GX51) and a scanning electron microscope (Tescan VEGA 3 LMH). Energy-dispersive X-ray microanalysis of local microvolumes in the irradiated alloy layers was performed using a Tescan VEGA 3 LMH scanning electron microscope equipped with a Bruker XFlash 5010 SSD EDS detector. The distribution of alloying elements across the cross-section was determined using mapping mode on a Tescan VEGA 3 LMH scanning electron microscope using energy-dispersive X-ray analysis method. To reveal the granular microstructure of the craters, the surface was chemically etched using Keller's etchant.

RESULTS AND DISCUSSION

The effect of HCPEB irradiation on materials comprises mechanical, thermal, and radioactive effects [1,11]. Under such irradiation, the alloy's heating rate is higher in the deeper layers. Maximum energy absorption occurs at a depth of approximately one-third of the electron path length in this material. This results in an explosive ejection of molten material and the subsequent rapid cooling of the alloy via heat transfer to the target's bulk. Cooling is accompanied by the crystallization of the molten material and structural and phase transformations. Previous studies [3, 23] have examined the characteristics of structural and phase changes in the surface layer of the HCPEB-irradiated AA6111 industrial aluminum alloy (Al-Mg-Cu-Si system). In particular, it was determined that the effect of HCPEB is accompanied by the formation of a complex surface topography on the AA6111 alloy plate and the appearance of microcracks and craters on its surface. The surface exhibits a wavy texture with localized protrusions exceeding 100 μm in height. The presence of these hemispherical protrusions is caused by the ejection of molten material from the area of maximum energy release and the ultrarapid solidification of the molten material following irradiation. The local surface roughness does not exceed 1.7 μm. At the same time, the depth of the surface-modified layer reaches 200 μm.

Fig. 1 shows a panoramic micrograph of the crater distribution on the irradiated surface of a target made of AA6111 alloy. An analysis of these micrographs revealed that the craters are distributed fairly uniformly across the entire irradiated surface. Most craters are either perfectly round or elliptical. A visual inspection of the irradiated surface confirms that most craters appear exactly as shown in Fig. 1.

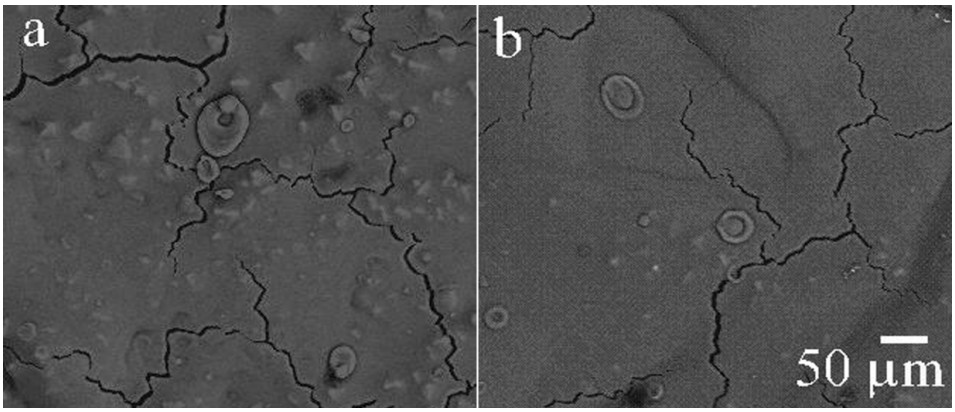

Figure 1. Appearance of craters on an irradiated target of AA6111 alloy: a and b are different areas of the irradiated surface

Fig. 2 shows an overview of the diameters of several craters, which vary significantly in size, for a more detailed analysis of their appearance. Thus, the diameter of the crater shown in Fig. 2a is approximately 100 μm, the diameter of the crater shown in Fig. 2b is approximately 65 μm, and the diameter of the crater shown in Fig. 2c is approximately 10 μm. That is, the diameters of the largest and smallest craters in Fig. 2 differ by an order of magnitude. An analysis of the overall appearance of all three craters shown in Fig. 2 suggests that the craters formed on the HCPEB-irradiated surface of the AA6111 alloy are characterized by central symmetry. Craters are typically multi-ringed and have a funnel-like morphology. The craters either have a distinct ring structure (see Fig. 2a) or feature blurred peripheral rings (see Fig. 2bc). The larger the crater's diameter, the more ring-like structures it has. The crater floor can be either flat, as in the crater shown in Fig. 2b; or parabolic, as in the crater shown in Fig. 2a. The edge of a crater is usually higher than the average surface level, while its center is lower.

The distribution of craters by size is an important parameter that can be quantified. Such data are of particular interest in predicting the mechanism of crater formation, which has not yet been fully studied and remains debatable [12,17-19]. To establish this relationship, the diameters of the craters were measured in two mutually perpendicular directions, and the average was calculated. The statistical results of a quantitative analysis of micrographs of craters on the irradiated

surface are shown in Fig. 3. The block diagram shows the distribution of craters by size, expressed as percentages. It is evident that the resulting distribution of crater sizes is approximately Gaussian. It is also evident that most craters range in size from 20 μm to 50 μm, and that the average diameter of all craters, D, is 37 μm. Measuring the crater density n and the average crater size D allows determining the crater coverage ratio of the HCPEB-treated surface $S = \pi D^2 n/4$ [17]. This parameter is an important factor in determining the degree to which craters occupy the surface area of a HCPEB-modified surface and, as such, may be significant in determining certain properties of surfaces treated in this manner. The calculated value of S for the irradiated surface of the AA6111 alloy is 3.7%. That is, the craters occupy a negligible portion of the alloy's irradiated surface. However, based on the value of S, the presence of craters shall be taken into account when analyzing the physical and technological properties of the irradiated surface.

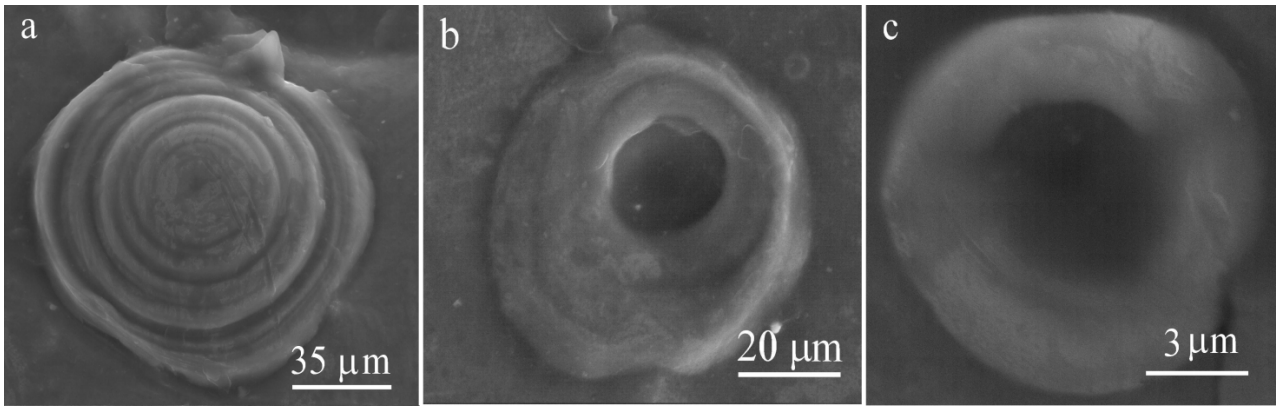

Figure 2. Appearance of craters on an irradiated target of AA6111 alloy

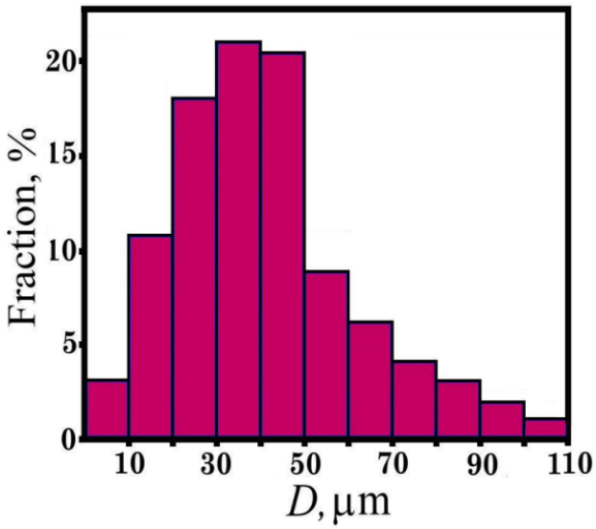

Figure 3. Size distribution of craters on an irradiated target of AA6111 alloy

It is known that chemical composition is an important indicator of a metal's structure following HCPEB treatment. Therefore, an analysis of the chemical composition was conducted on the crater walls and on the remelted surface adjacent to the crater. The studies were conducted on the crater shown in Fig. 4. Fig. 4c shows the EDS testing areas (labeled 1, 2, and 3). Data on the chemical composition of the selected areas are shown in Table 1. Each value shown in this table is an average value for the selected areas. An analysis of the data in Table 1 allows for the drawing of several conclusions about the chemical composition of the spectra studied. First and foremost, there are noticeable differences in the Mg and O content across the selected areas. Given the characteristic ratio of the mass fractions of oxygen and magnesium, it can be concluded that an oxide film consisting of MgO is present on the surface of the remelted layer. Irradiation was done by a single impulse in a vacuum at 1.3×10^{-3} Pa. At this pressure, oxidation will still occur due to the presence of oxygen in the residual vacuum. Magnesium oxidizes much more rapidly in the air than aluminum does. Magnesium oxide is easier to form than Al_2O_3, as magnesium is more reactive than aluminum. MgO is the initial product of the oxidation of a molten magnesium-containing aluminum alloy [26]. As for the other alloying elements present in the AA6111 alloy, there are minor differences in their distribution between the alloy's surface layer and the inner walls of the craters. In addition, the concentrations of Cu and Si on the inner walls of the crater are slightly higher than in the central part of the crater.

Fig. 4b shows the results of studies on the distribution of Mg atoms across the irradiated surface, conducted in mapping mode. Magnesium is distributed in patches over the surface. Thus, the differences in magnesium content in the

spectrum are due to the patchy distribution of magnesium oxide over the surface, as shown in Fig. 4b. At the same time, the distribution of aluminum atoms on the irradiated surface is more uniform (see Fig. 4a) than that of magnesium atoms. It should be noted that similar studies were conducted in [27] using an Al-20%Si-5%Mg alloy as an example. This study also highlights that aluminum atoms are distributed more uniformly in the crater area than are Si and Mg atoms. The highest concentration of Si and Mg atoms was found at the crater floor [27]. At the same time, according to the energy-dispersive analysis data (Table 1), the central region of the crater was depleted in magnesium and silicon.

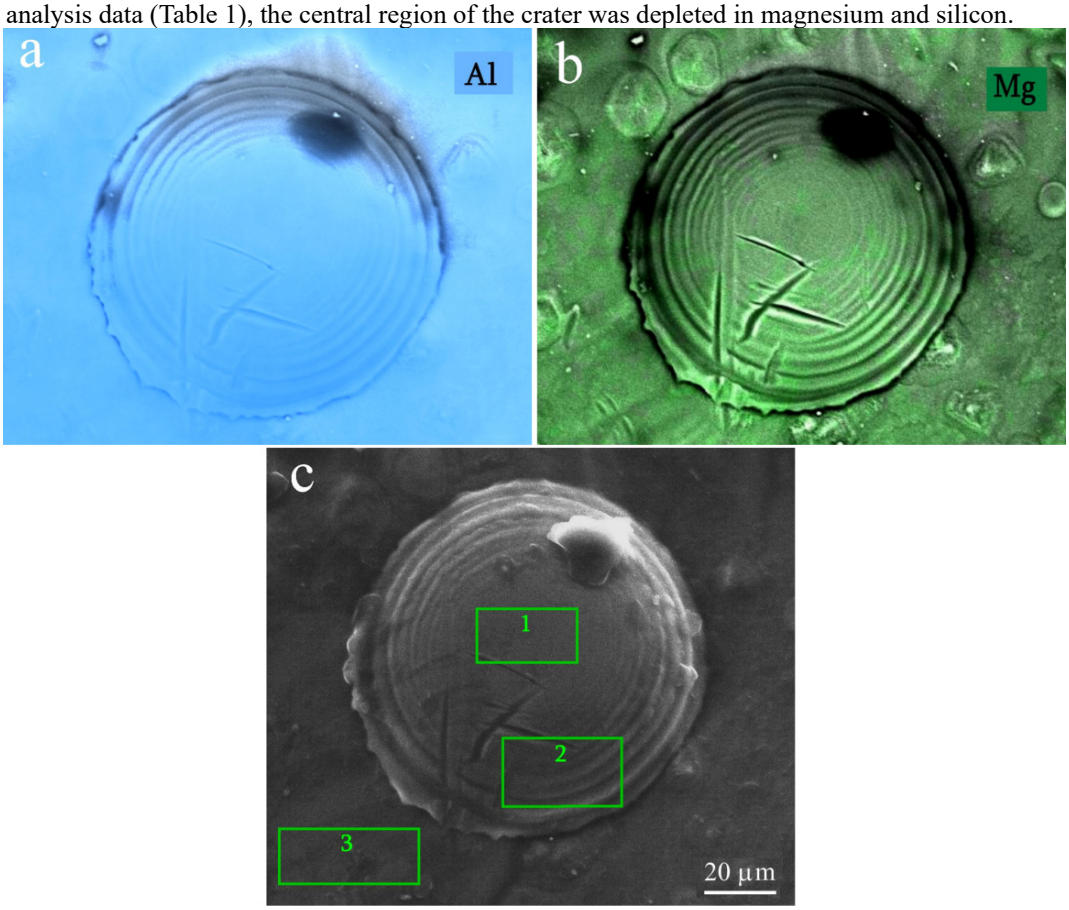

Figure 4. SEM image of a crater on the surface of the remelted alloy layer. Maps showing the distribution of magnesium (b) and aluminum (a) atoms across the surface

Table 1. EDS Analysis Results of Selected Areas in Fig. 4(c)

Spectrum	O	Mg	Al	Si	Mn	Fe	Cu
1	1.61	0.87	98.70	0.13	0.04	0.07	0.20
2	2.82	1.09	95.15	0.41	0.05	0.21	0.27
3	3.27	1.43	94.25	0.32	0.06	0.09	0.28

As shown in [28], crater formation alters the local stress state. Heterogeneity in the stress state can affect the appearance and shape of the grain structure in the vicinity of the crater formed during melt solidification. Fig. 5a shows the grain structure of the irradiated surface of the AA6111 alloy under study in the area where the crater is located. Asymmetrical, elongated grains, radiating outward from the central eruption zone, are visible near the center of the crater. Whereas smaller equiaxial grains are observed at the crater's rim. All of this suggests that solidification occurred quickly after the eruption that formed the crater. Thus, crater formation affects the course of the melt crystallization process and, consequently, the physical and technological properties of the surface after irradiation. A similar crater grain structure in type and shape was also observed in study [29]. Fig. 5b shows the granular microstructure on the surface away from the craters. An equiaxial, uniform microstructure is observed, which may indicate that the surface has uniform physical and technological properties and contains no craters. Thus, the craters introduce distortions in the surface properties of the HCPEB-irradiated surface.

Since craters significantly impact the surface properties of materials exposed to pulsed energy beams, understanding the mechanisms of crater formation is crucial for understanding the fundamental processes involved in HCPEB irradiation and, consequently, for predicting the potential applications of this technology. According to [17], non-uniform local melting in the near-surface layer of the target material, followed by the ejection of molten material through the solid outer surface, is the primary hypothesis for the crater formation. An alternative mechanism suggests that craters form due to uneven crystallization of the remelted layer [19]. Arguments in favor of one or another mechanism of crater formation during irradiation are crucial for further understanding the processes that occur when materials are irradiated with HCPEB.

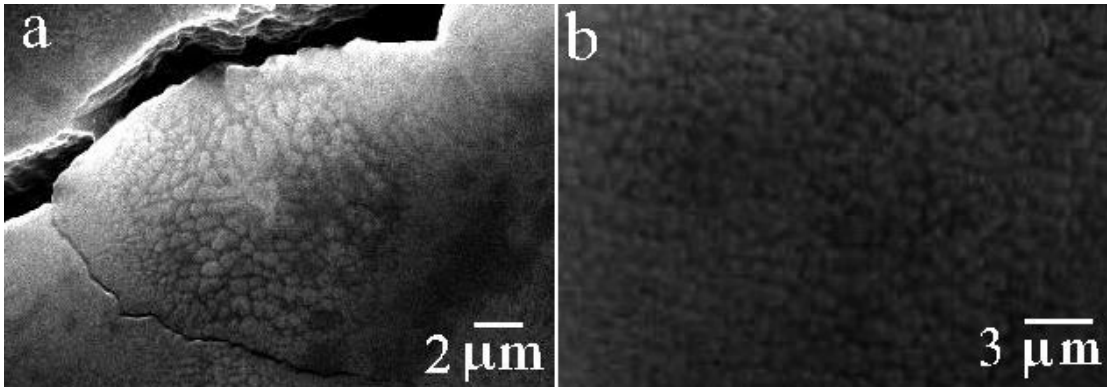

Figure 5. Appearance of the grain microstructure in the crater location area of an irradiated target of AA6111 alloy (a); general appearance of the grain microstructure on the irradiated surface of the AA6111 alloy (b)

It is known that the presence of surface cracks is a characteristic feature of many aluminum alloys and other metals and alloys irradiated with HCPEB [2,3,5,30]. As shown in Fig. 1 and Fig. 6, such cracks are also present on the irradiated surface of the AA6111 alloy under study. The zigzag-like pattern of cracks on the surface is caused by local inhomogeneities in the distribution of alloying elements within the solidified material and local variations in the strength and ductility properties of the solidified material across its various microvolumes. However, it is worth noting that some craters are crossed by fractures (see Fig. 6ab), whereas others lie atop fractures (see Fig. 6cd). In other words, some craters form during the crystallization of the molten layer, while others form after the surface layer has already crystallized. This may support the crater-formation mechanism proposed in [19], according to which craters form during crystallization of the molten target material due to uneven crystallization of the remelted layer.

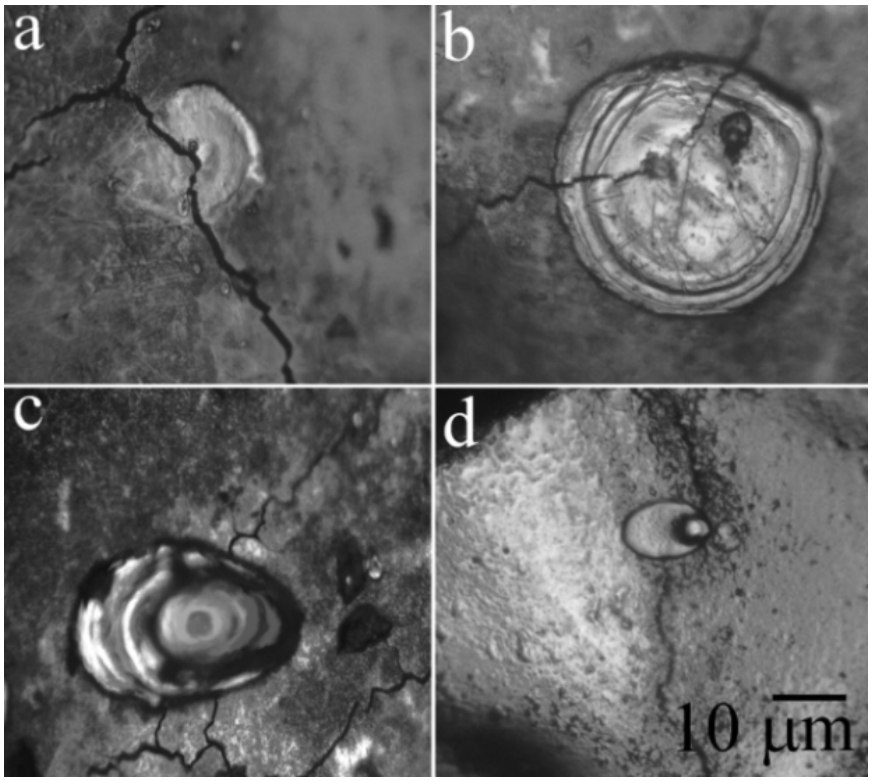

Figure 6. Appearance of craters on the irradiated surface of AA6111 alloy

CONCLUSIONS

It has been shown that HCPEB irradiation with a particle energy of 0.35 MeV, a beam current of 2.0 kA, a pulse duration of 5 μs, and a beam diameter of 3 cm results in the formation of craters on the surface of the AA6111 industrial aluminum alloy.

The craters are distributed fairly evenly across the entire irradiated surface of the AA6111 alloy target, and the size distribution of the craters, as a function of their fractional abundance, follows an approximately Gaussian distribution. Most craters range in size from 20 μm to 50 μm.

There is a non-uniform distribution of alloying elements in the alloy's surface layer and on the inner crater walls. The concentrations of Cu and Si on the inner crater walls are slightly higher than in the central part of the crater.

The grain structure of the irradiated surface in the crater region was studied. It has been established that asymmetrically elongated grains are observed near the crater center, radiating outward from the central eruption zone.

The overall appearance of the irradiated surface of the AA6111 alloy indicates that craters form during crystallization of the molten target material due to uneven remelting of the layer.

ORCID

Vasyl Bryukhovetsky, https://orcid.org/0000-0003-0423-8828; **Volodymyr Lytvynenko,** https://orcid.org/0000-0003-4850-2555
Diana Myla, https://orcid.org/0000-0003-2919-741X; **Oleg Rak,** https://orcid.org/0009-0000-6683-1235

REFERENCES

[1] Y. Qin, C. Dong, Z. Song, S. Hao, X. Me, J. Li, X. Wang, J. Zou, and Th. Grosdidier, J. Vacuum Sci. and Technol. A, **279**(3), 430 (2009). https://doi.org/10.1116/1.3093876
[2] V.V. Bryukhovetsky, V.F. Klepikov, V.V. Lytvynenko, D.E. Myla, V.P. Poyda, A.V. Poyda, V.T. Uvarov, *et al*., Nucl. Instrum. Methods Phys. Res. Sect. B, **499**, 25 (2021). https://doi.org/10.1016/j.nimb.2021.02.011
[3] V.V. Bryukhovetsky, V.F. Klepikov, V.V. Lytvynenko, D.E. Myla, Yu.F. Lonin, and A.G. Ponomarev, Nucl. Instrum. Methods Phys. Res. Sect. B. **519**, 1 (2022). https://doi.org/10.1016/j.nimb.2022.03.008
[4] H. Xie, J. Cai, C. Yu, M. Feng, X. Li, S. Chen, W. Pu, *et al*., Journal of Alloys and Compounds, **1025,** 180201 (2025). https://doi.org/10.1016/j.jallcom.2025.180201
[5] D.E. Myla, V.V. Bryukhovetsky, V.V. Lytvynenko, V.P. Poyda, A.V. Poyda, V.F. Klepikov, V.T. Uvarov, *et al*., Problems of Atomic Science and Technology, **2**(126), 33 (2020).
[6] Y. Hao, B. Gao, G.F. Tu, S.W. Li, C. Dong, and Z.G. Zhang, Nucl. Instrum. Methods Phys. Res. Sect. B, **269**, 1499 (2011). https://doi.org/10.1016/j.nimb.2011.04.010
[7] V.V. Bryukhovetsky, A.V. Poyda, V.P. Poyda, and D.E. Milaya, Problems of Atomic Science and Technology, **2**(120), 67 (2019).
[8] V.V. Bryukhovetsky, V.V. Lytvynenko, D.E. Myla, V.A. Bychko, Yu.F. Lonin, A.G. Ponomarev, and V.T. Uvarov, Physics and Chemistry of Solid State, **22**, 655 (2021), https://doi.org/10.15330/pcss.22.4.655-663
[9] J. Cai, L. Ji, S.Z. Yang, X.T. Wang, Y. Li, X.L. Hou, and Q.F. Guan, Chinese Science Bulletin, **58**, 2507 (2013). https://doi.org/10.1007/s11434-013-5848-5
[10] V.V. Bryukhovetsky, V.V. Lytvynenko, O.A. Startsev, D.E. Myla, Yu.N. Volkov, and O.L. Rak, Materials Letters, **367**, 136642 (2024). https://doi.org/10.1016/j.matlet.2024.136642
[11] D.I. Proscurovsky, and A.D. Pogrebnjak, Phys. Stat. Sol. A, **145**(1), 9 (1994). https://doi.org/10.1002/pssa.2211450103
[12] V.V. Bryukhovetsky, V.V. Lytvynenko, Yu.F. Lonin, D.E. Myla, A.G. Ponomarev, and V.T. Uvarov, Problems of Atomic Science and Technology, **2**(144), 24 (2023). https://doi.org/10.46813/2023-144-024
[13] C. Zhang, Y. Zhang, N. Tian, S. Chen, Z. Qian, P. Lv, and Q. Guan, Protection of Metals and Physical Chemistry of Surfaces, **52**, 869 (2016). https://doi.org/10.1134/S2070205116050269
[14] Z. Zhang, S. Yang, P. Lv, Y. Li, X. Wang, X. Hou, and Q. Guan, Applied surface science, **294**, 9 (2014). https://doi.org/10.1016/j.apsusc.2013.12.178
[15] L. Chai, B. Chen, S. Wang, Z. Zhang, and K.L. Murty, Applied Surface Science, **390**, 430 (2016). https://doi.org/10.1016/j.apsusc.2016.08.128
[16] J. Cai, Q. Guan, P. Lv, C. Zhang, and Y. Yin, High Temperature Materials and Processes, **37**(8), 777 (2018). https://doi.org/10.1515/htmp-2017-0067
[17] Y. Qin, Ch. Dong, X. Wang, Sh. Hao, A. Wu, J. Zou, and Y. Liu, J. of Vacuum Science & Technology A, **21**(6), 1934 (2003). https://doi.org/10.1116/1.1619417
[18] J. Zhang, X. Zou, T. Grosdidier, C. Dong, J. of Vacuum Sci. & Technol. A, **27**, 1217 (2009). https://doi.org/10.1116/1.3207948
[19] V.V. Bryukhovetsky, V.F. Klepikov, V.V. Lytvynenko, D.E. Myla, O.A. Startsev, Yu.F. Lonin, and A.G. Ponomarev, Vacuum, **215**, 112263 (2023). https://doi.org/10.1016/j.vacuum.2023.112263
[20] P.E. Fortin, M.J. Bull, and D.M. Moore, SAE Int. Congr. Exp., Detroit, MI, 1983, SAE Paper no. 830096. https://doi.org/10.4271/830096
[21] V.V. Bryukhovetskyy, V.P. Pojda, A.V. Poyda, D.R. Avramets', R.I. Kuznetsova, O.P. Kryshtal', O.L. Samsonnik, *et al*., Metallofiz. Noveishie Tekhnol. **31**(9), 1289-1302 (2009).
[22] G.K. Quainoo, S. Yannacopoulos, and A.K. Gupta, Canadian Metallurgical Quarterly, **40**(2), 211 (2001). https://doi.org/10.1179/000844301794388515
[23] D.E. Myla, V.V. Bryukhovetsky, V.V. Lytvynenko, S.I. Petrushenko, O.O. Nevgasimov, Yu.F. Lonin, A.G. Ponomarev, *et al*., Problems of Atomic Science and Technology, **2**(138), 25 (2022). https://doi.org/10.46813/2022-138-025
[24] V.V. Bryukhovetskij, Fizika Metallov i Metallovedenie, **92**(1), 107 (2001). (in Russian)
[25] V.V. Bryukhovetsky, S.E. Donets, S.A. Kniaziev, O.V. Subbotin, V.V. Lytvynenko, S.I. Bogatyrenko, O.L. Rak, *et al*., Problems of Atomic Science and Technology, **6**(160), 76 (2025). https://doi.org/10.46813/2025-160-076
[26] K. Kim, Surface and Interface Analysis, **47**(4), 429 (2015). https://doi.org/10.1002/sia.5726
[27] B. Gao, K. Li, and P. Xing, Coatings, **9**(7), 413 (2019). https://doi.org/10.3390/coatings9070413
[28] P. Yan, T. Grosdidier, X. Zhang, and J. Zou, Materials & Design, **159**, 1 (2018). https://doi.org/10.1016/j.matdes.2018.08.033
[29] J. Zou, T. Grosdidier, K. Zhang, and C. Dong, Acta Materialia, **54**(20), 5409 (2006). https://doi.org/10.1016/j.actamat.2006.05.053
[30] V.V. Bryukhovetsky, V.V. Lytvynenko, D.E. Myla, Yu.F. Lonin, A.G. Ponomarev, and V.T. Uvarov. J. Nano- and Electronic Physics, **13**(6), 06025-1 (2021). https://doi.org/10.21272/jnep.13(6).06025

МОРФОЛОГІЧНІ ОСОБЛИВОСТІ ТА ХАРАКТЕРИСТИКИ МІКРОСТРУКТУРИ КРАТЕРІВ НА ОПРОМІНЕНІЙ СИЛЬНОСТРУМОВИМ ІМПУЛЬСНИМ ПУЧКОМ ЕЛЕКТРОНІВ ПОВЕРХНІ ПРОМИСЛОВОГО АЛЮМІНІЄВОГО СПЛАВУ AA6111

В.В. Брюховецький[1], В.В. Литвиненко[1], Д.Є. Мила[1], О.Л. Рак[2]

[1]Інститут електрофізики і радіаційних технологій НАН України, вул. Гуданова, 13, 61024 Харків, Україна
[2]ННЦ «Харківський фізики-технічний інститут» НАН України, вул. Академічна, 1, 61108 Харків, Україна

Опромінення промислового алюмінієвого сплаву AA6111 сильнострумовим імпульсним електронним пучком з енергією частинок 0,35 МеВ, струмом пучка 2,0 кА, тривалістю імпульсу 5 мкс та діаметром пучка 3 см призводить до формування поверхневого шару з покращеними фізико-технологічними властивостями. Однак одним із негативних ефектів, спричинених імпульсним електронним опроміненням, є потенційне утворення кратерів на поверхні опроміненого матеріалу. В роботі вивчені типи та морфологія кратерів на поверхні алюмінієвого сплаву AA6111, що виникають внаслідок опромінення поверхні цього сплаву. Вивчено розподіл кратерів за розмірами та щільність кратерів на опроміненій поверхні. Проведено аналіз складу хімічних елементів на поверхні стінок кратера та на прилеглій до кратера переплавній поверхні. Вивчено особливості форми та розмірів мікроструктури зерен у зоні розташування кратера. Обговорюється значення цих спостережень для глибшого розуміння механізмів утворення кратерів під час опромінення сильнострумовим імпульсним електронним пучком.

Ключові слова: с*ильнострумовий імпульсний електронний пучок; алюмінієвий сплав, поверхневий шар; кратери*